PhenoChip: A single-cell phenomic platform for high-throughput photophysiological analyses of microalgae

Author(s):
Behrendt, Lars; Salek, M. Mehdi; Trampe, Erik L.; Fernandez, Vicente I.; Lee, Kang Soo; Kühl, Michael; Stocker, Roman

Publication date:
2020-09-02

Permanent link:
https://doi.org/10.3929/ethz-b-000441496

Originally published in:
Science Advances 6(36), https://doi.org/10.1126/sciadv.abb2754

APPLIED ECOLOGY

PhenoChip: A single-cell phenomic platform for high-throughput photophysiological analyses of microalgae

Lars Behrendt[1,2]*, M. Mehdi Salek[1,3], Erik L. Trampe[4], Vicente I. Fernandez[1], Kang Soo Lee[1], Michael Kühl[4], Roman Stocker[1]*

Photosynthetic microorganisms are key players in aquatic ecosystems with strong potential for bioenergy production, yet their systematic selection at the single-cell level for improved productivity or stress resilience ("phenotyping") has remained largely inaccessible. To facilitate the phenotyping of microalgae and cyanobacteria, we developed "PhenoChip," a platform for the multiparametric photophysiological characterization and selection of unicellular phenotypes under user-controlled physicochemical conditions. We used PhenoChip to expose single cells of the coral symbiont *Symbiodinium* to thermal and chemical treatments and monitor single-cell photophysiology via chlorophyll fluorometry. This revealed strain-specific thermal sensitivity thresholds and distinct pH optima for photosynthetic performance, and permitted the identification of single cells with elevated resilience toward rising temperature. Optical expulsion technology was used to collect single cells from PhenoChip, and their propagation revealed indications of transgenerational preservation of photosynthetic phenotypes. PhenoChip represents a versatile platform for the phenotyping of photosynthetic unicells relevant to biotechnology, ecotoxicology, and assisted evolution.

INTRODUCTION

Photosynthesis is regulated via protein modifications, changes in gene regulation, biophysical adjustments of photosystems, and variations in morphology in response to environmental conditions that ultimately result in a distribution of phenotypes with different photosynthetic performance within populations. The selection of phototrophs based on their phenotype ("phenomics") has a long history, and crops, in particular, have been selected for important agronomic traits over the course of human history. Technical advances in high-throughput plant phenomics and genetics have accelerated the pace of crop improvement, and selection under controlled dynamic environments has proven fundamental for the discovery of "emergent phenotypes" that are not evident under steady-state conditions and appear critical for plant responses to environmental perturbations (*1*). In contrast, the phenomic investigation of unicellular photosynthetic organisms (microalgae and cyanobacteria) is still in its infancy, despite the key ecological importance of these organisms in aquatic ecosystems and their potential for bioproduction of food, chemicals, fuels, and other materials.

Microalgae and cyanobacteria inhabit dynamic environments and have evolved diverse physiological traits under a complex continuum of niche-defining selective forces (*2*). Optimal acquisition and photosynthetic processing of light energy is key to their survival under fluctuating temperature, irradiance, pH, and availability of nutrients. The principal goal of this photosynthetic "fine tuning" is the protection of the photosynthetic machinery while meeting cellular energy requirements. This can result in the appearance of a range of appropriate photophysiologies under specific environmental conditions. Selecting these phenotypes would be of clear value in applications that exploit unicellular phototrophs, but currently, there is a lack of a suitable experimental platform to enable rapid, high-throughput phenotyping of microalgae and cyanobacteria based on their photosynthetic performance under relevant environmental conditions.

Here, we describe "PhenoChip," a compact and versatile microfluidic device for microalgal phenomics. In its current configuration, the device integrates several functions into a microfluidic chip, i.e., it delivers chemical gradients to immobilized cells by diffusively mixing solutes within a microchannel network (a "Christmas tree gradient generator") located upstream of the microwell array, and creates temperature gradients by applying electrical currents to a conductive path adjacent to the microwell array (*3*). Without further modifications, the array of immobilized cells within PhenoChip can also be exposed to other physicochemical gradients (e.g., gas and light). Essential to the selection of cells on the basis of their phenotype is the ability to propagate or further interrogate specific cells after a defined experimental treatment. In PhenoChip, the removal of immobilized cells is achieved by ejecting cells from their individual microwell via optical methods (laser dissection). This allows cells to be seized at the outlet of PhenoChip and to be used in subsequent experiments or cultivation. In combination, these techniques enable high-throughput phenotyping of individual unicellular phototrophs under controlled microenvironmental conditions. With the current configuration of the microwell array, PhenoChip is compatible with phototrophic fractions of nanophytoplankton (2 to 20 μm) and microplankton (20 to 200 μm), two important size classes within aquatic environments and the dominant size classes for biotechnologically relevant microalgae. Other devices allow for the selection and isolation of single microalgae (*4*) as well as their exposure to controlled conditions for extended time periods (*5*), yet none in concert with each other and specifically for single-cell phenotyping.

In a first proof-of-concept demonstration, we used PhenoChip to study the photophysiology of *Symbiodinium* (Symbiodiniaceae), a genus of microalgae that often engages in symbiosis with corals and other marine animals but can also be free living (*6*). As a symbiont that can

[1]Institute of Environmental Engineering, Department of Civil, Environmental and Geomatic Engineering, Eidgenössische Technische Hochschule Zürich (ETHZ), Stefano-Franscini-Platz 5, 8093 Zürich, Switzerland. [2]Science for Life Laboratory, Department of Environmental Toxicology, Uppsala University, Norbyv. 18A, 75236 Uppsala, Sweden. [3]School of Engineering, Massachusetts Institute of Technology, 77 Massachussetts Ave., MA 02139, USA. [4]Marine Biological Section, Department of Biology, University of Copenhagen, Strandpromenaden 5, DK-3000 Helsingør, Denmark.
*Corresponding author. Email: lars.behrendt@scilifelab.uu.se (L.B.); romanstocker@ethz.ch (R.S.)

supply its coral host with >70% of its energy demand, *Symbiodinium* is crucial for the health and resilience of coral reefs. Reefs are now under pressure, in large part due to frequent and severe coral bleaching events provoked by climate change, whereby *Symbiodinium* disappears (through an essentially unknown mechanism) from the coral tissue due to thermal stress (*7*), and weakening of their capability to deposit calcium carbonate, i.e., the framework of the reef, driven by ocean acidification (*8*). Bleached corals do not decease immediately without photosymbionts and, importantly, can reestablish symbiotic relationships with more stress-tolerant *Symbiodinium* types from the environment (*9*). In the coral research community, the need has thus been expressed for new mitigation strategies, to "develop coral stocks with enhanced stress tolerance" (*10*). As part of this strategy, cultivars of *Symbiodinium* have undergone experimental evolution, which, in certain cases, has resulted in increased growth rates and photosynthetic efficiencies at higher temperatures (*11*). Other proposed strategies include the targeted (e.g., via genetic engineering) or untargeted (random mutagenic) manipulation of *Symbiodinium* genomes, followed by selection of phenotypes with increased stress tolerance (*10*). However, these approaches seldom take into account the phenotypic heterogeneity among single cells within and between *Symbiodinium* strains, which, in the context of phenotyping, is of importance as it might reveal genotypes within populations that better resist environmental fluctuations (*12*).

Here, we investigated two *Symbiodinium* strains, the symbiotic strain CCMP2467 [clade A1, *Symbiodinium microadriaticum* (*6*)] and the nonsymbiotic, free-living strain CCMP421 [clade E, *Effrenium voratum* (*6*)], for their ability to withstand short-term environmental perturbations typical of the onset of coral bleaching. Immobilized single cells from both strains were exposed to periodic up- and downshifts of progressively increasing temperatures and, in separate experiments, to a gradient of pH. Single-cell photophysiological responses were concurrently measured using pulse amplitude–modulated chlorophyll fluorometry (PAM) imaging, resulting in a direct coupling of time-resolved measurements of the effective (Φ_{II}) and maximal (F_v/F_m) photosystem (PS) II quantum yields in response to environmental stimuli. Here, F_v/F_m evaluates the maximum efficiency of PSII in darkness, while Φ_{II} estimates the operating efficiency under actinic light. We present the first photophenomic assessment of two strains of *Symbiodinium* and highlight the power of PhenoChip to uncover their single-cell population heterogeneity, photosynthetic stress tolerance, and recovery. We suggest that this approach provides a versatile platform for the phenotyping of photosynthetic unicells relevant to biotechnology and ecotoxicology and a powerful tool in assisted evolution strategies.

RESULTS

PhenoChip combines single-cell immobilization and delivery of physicochemical gradients with imaging of photophysiological performance. To enable high-throughput quantification of the performance of photosynthetic unicells, PhenoChip (Fig. 1) contains a high-density array of geometrically arranged microwells (>29,000 per chip), into which cells are loaded via gravitational deposition and compression of the microfluidic channel surrounding the wells. The passive confinement of cells in microwells is particularly attractive due to the relative simplicity of fabricating and loading wells, the high cell occupancy rates, and the ability to retain cells for extended durations (>7 days have been achieved). By integrating microwells into a microfluidic device, immobilized individual cells can be exposed to precisely controlled gradients of physicochemical stimuli while observing them via microscopy techniques. In contrast to other droplet-based microfluidic platforms used in single-cell phenotyping [e.g., Ohan *et al.* (*13*)], PhenoChip can observe the response of the same cell to a range of physicochemical

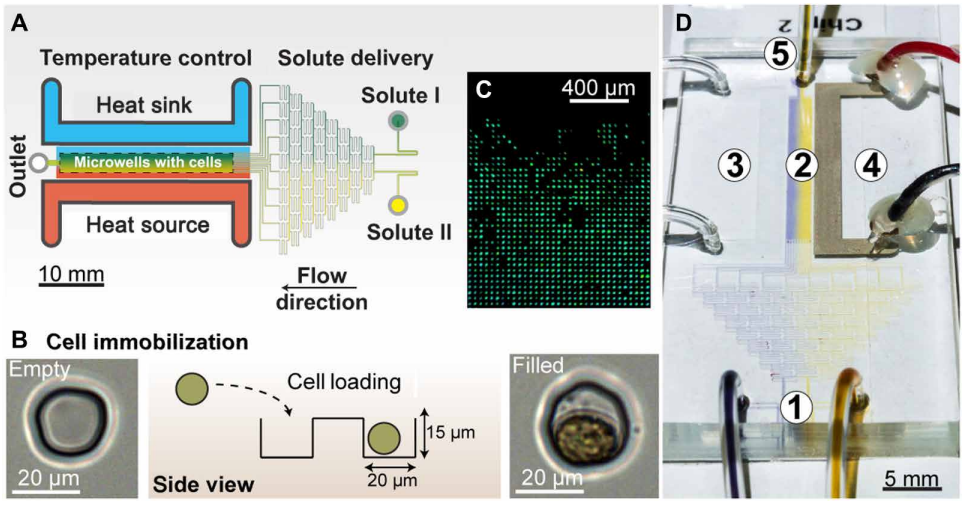

Fig. 1. PhenoChip, a microfluidic platform that integrates single-cell immobilization and delivery of physicochemical gradients with photophysiological imaging. (**A**) Schematic of the PhenoChip microfluidic device, composed of three principal design elements for cell immobilization, generation of temperature gradients, and generation of chemical gradients. Cells are immobilized individually within the main channel (width, 2.28 mm; height, 75 µm; length, 20.5 mm) in an arena of approximately 29,000 microwells. (**B**) In the main channel, the microwells (here, 20-µm diameter, 15-µm depth) are seeded with cells using gravitational deposition followed by slight compression of the flexible PDMS device. Loading can be confirmed by light microscopy (left, empty microwell; right, microwell containing a single microalgal cell). (**C**) For noninvasive, real-time photophysiological imaging of single cells, PhenoChip is coupled to a variable chlorophyll fluorescence imaging microscope (PAM). The image shows a PAM-derived, false-color image of quantum yields of immobilized single microalgal cells within a portion of the microwell array comprising ca. 1500 wells. (**D**) Photographic image of PhenoChip with colored solutes injected into both inlet ports (1) and the resulting gradient across the microwell arena (2). Temperature sink (3) and source (4) channels as well as the outlet (5) are shown with their respective transparent tubing or electrically conductive wires (black/red).

perturbations over time. To facilitate continuous measurement, cells taken from a well-mixed culture were immobilized in microwells located within a main microchannel (Fig. 1, A and D), where they are continuously supplied with media and, if desired, gradients of solutes provided via a microfluidic gradient generator (Fig. 1, A and D). This immobilization does not affect cell physiology (fig. S1) and neither does flow-induced shear stress (fig. S2). To directly observe the effect of controlled physicochemical conditions on photosynthetic cells, PhenoChip can be mounted onto a variable chlorophyll fluorescence imaging system, allowing noninvasive cell-specific readout of the PSII quantum yield (Fig. 1C) under dark conditions, F_v/F_m, or under a given actinic irradiance, Φ_{II}. The throughput of PhenoChip is principally determined by the magnification of the chlorophyll fluorescence imaging system and whether continuous or single readouts of F_v/F_m or Φ_{II} are acquired. For continuous measurements under temperature perturbations, the throughput is approximately 220 cells hour^{-1}, assuming 1000 cells per field of view and an experimental duration of 5 hours. The throughput for single readouts is much higher at approximately 500 cells min^{-1}, assuming 1000 cells per field of view and a measurement duration of 90 s per field of view and a travel duration of 30 s between fields of view.

Generating temperature gradients in PhenoChip

PhenoChip allows the dynamic application of varying temperatures to immobilized cells. To provide accurate temperature control, a thermal source channel adjacent to the main channel containing the microwells is filled with a low-conductive polymer and connected to a power source (Fig. 1, A and D). This is an established method for providing temperature gradients in microfluidics (*3*) and permits the dynamic manipulation of temperature by simple regulation of electric current (Fig. 2A). In PhenoChip, the relation between input current and resulting temperature is linear (adjusted $R^2 = 0.94$; fig. S3) and can be modulated to achieve stepwise temperature increases of +1°C in the center of the main channel (Fig. 2B, dotted line). Computational fluid dynamic (CFD) modeling and validation experiments confirmed the linear change in temperature across the width of the channel and allowed the accurate quantification of the temperatures experienced by individual cells within each of the 57 rows of microwells (Fig. 2, A and B, and table S1) or, more coarsely, by consolidating groups of 10 rows of microwells into six "temperature bins" (Fig. 2B).

Comparing the response of *Symbiodinium* strains to rising temperatures

Photosynthetic cells, including *Symbiodinium*, are particularly sensitive to rising temperature, which can alter their ability to photosynthesize by affecting, for example, the stability of the constituents of PSII and repair processes (*14*). To evaluate the direct effect of transient, moderate heat stresses of different magnitudes on F_v/F_m the same single cells were exposed to five consecutive heating periods of 360 s (Fig. 2C, numbered 1 to 5 in Fig. 3, A and B), each separated by a cooling period of 360 s (white spaces, Fig. 3, A and B). The combination of one heating period followed by a cooling period is referred to as a "thermal cycle" (duration = 720 s, Fig. 2C). Cells were sequentially exposed to five thermal cycles at a temperature of +1°C (Fig. 2B, light green), and the process was repeated for +2°, +3°, and + 4°C (five cycles each; Fig. 2B). A set of five thermal cycles with the same temperature is hereafter referred to as a "temperature treatment." Cells were allowed a recovery period of 28.5 min without heating immediately after the +3°C temperature treatment and before the +4°C treatment (Fig. 3, A and B). During each thermal cycle, eight measurements of F_v/F_m were performed at equally spaced time intervals (90 s; Fig. 2C, arrows). In a separate experiment, F_v/F_m was measured in cells that were kept at room temperature (RT) but otherwise monitored over the same experimental duration (Fig. 3, A and B). Probing photosynthesis at 90 s intervals reduced F_v/F_m by ~25% compared to

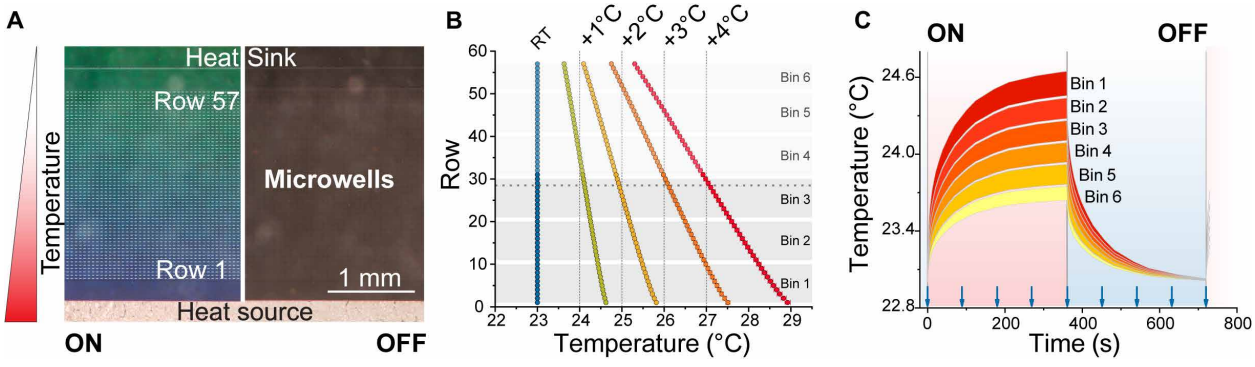

Fig. 2. PhenoChip enables the accurate application of thermal gradients. (**A**) Visual representation of temperature gradients within PhenoChip. Temperature gradients were visualized using temperature-sensitive liquid crystal (LC) sheets fixed to the glass microscope slide beneath the PhenoChip. Rows of microwells within PhenoChip (total $n = 57$) are indicated by horizontal lines. A gradient in color represents the gradient in temperature (green, low temperature; blue, high temperature) during the application ("'ON," left) and absence ("'OFF," right) of an electrical current. (**B**) CFD simulation of the temperature gradient across the 57 rows of microwells within PhenoChip, for five values of temperature (room temperature or "RT," +1°, +2°, +3°, and +4°C). Color-coded points represent average temperatures ± SD (smaller than symbol size) as computed from the simulation at steady-state conditions. The dotted horizontal line indicates the middle of the channel, where the reference integer temperature differences were obtained. Sets of ten rows of microwells were consolidated into a total of six bins (indicated by gray horizontal bars) for a coarse characterization of temperature effects. Note that the intrinsic magnification of the PAM camera system only allows for 31 rows of microwells to be measured simultaneously (bins 1 to 3, highlighted in dark gray) and that all data presented are derived from measurements performed on rows 1 to 31, on a total of 1500 microwells. (**C**) CFD simulation of a single thermal cycle within PhenoChip. A thermal cycle is characterized by the initial rapid elevation of temperatures during the application of an electrical current [ON; see (A)] and the rapid decrease of temperature in the absence of an electrical current (OFF). The resulting temperature variation over time is shown for the discretized microwell bins defined in (B). The PAM measurement interval (90 s) is indicated by blue arrows along the *x* axis.

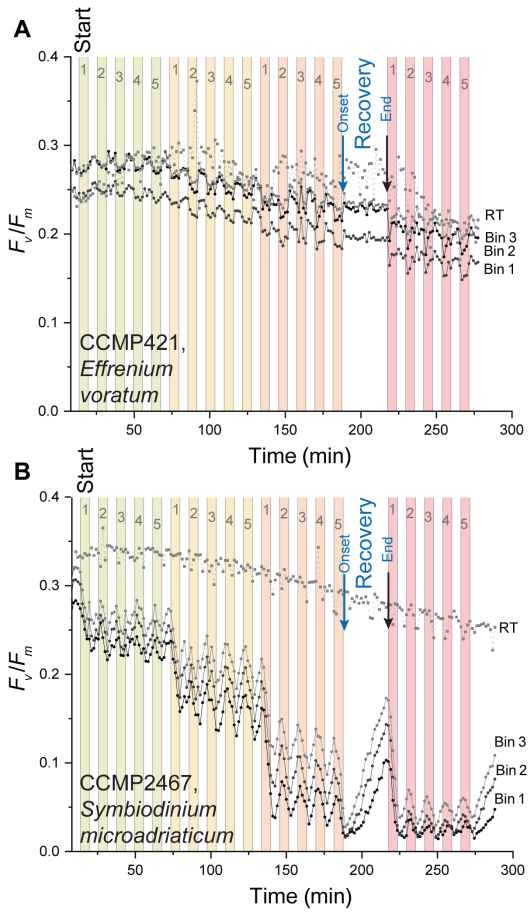

Fig. 3. PhenoChip enables the measurement of single-cell photophysiological responses to temperature, here demonstrated with two strains of *Symbiodinium sp.* (**A** and **B**) Maximum quantum yields (F_v/F_m) under repeated thermal cycling of incrementally increasing temperatures. Results are shown for *Symbiodinium* strains CCMP421 (A) and CCMP2467 (B). Curves represent average values of F_v/F_m for cells monitored at RT or within bins 1 to 3 during temperature experiments (as defined in Fig. 2B). In all experiments, cells were measured every 90 s using PAM in darkness. Cells in bins 1 to 3 were exposed to four temperature treatments (+1°, +2°, +3°, and +4°C), each consisting of five consecutive thermal cycles (sequentially numbered on colored bars), interspersed with five recovery periods (white bars). Cells were permitted a 28.5-min recovery period (Recovery) that started after the final cycle of the temperature treatment of +3°C, indicated by a blue arrow (Onset) and ended before the start of the next temperature treatment of +4°C, indicated by a black arrow (End).

initial values of F_v/F_m (fig. S4), and all experiments were started after the 10th saturation pulse (see the Supplementary Materials for additional discussion). All measurements of F_v/F_m were performed in the dark, without the application of actinic light, to evaluate the collective effect of heat stress on PSII activity and additional energy dissipation mechanisms.

The gradually increasing temperatures revealed a pronounced difference in the photophysiological response between *Symbiodinium* strain CCMP421 (Fig. 3A, $n = 564$, bins 1 to 3) and CCMP2467 (Fig. 3B, $n = 1056$, bins 1 to 3). The +1°C temperature treatment caused CCMP421 cells to increase their average value of F_v/F_m by a negligible +1% over average pre-exposure levels (consisting of the last four F_v/F_m before any temperature treatment), whereas cells from strain CCMP2467 decreased their average value by −17%. These differences persisted during exposure to higher temperatures; the temperature treatments of +2°, +3°, and +4°C caused average reductions in F_v/F_m relative to pre-exposure levels of respectively −4.8, −14, and −25% in CCMP421 and −31, −65, and −83% in CCMP2467. During the same measurement intervals, i.e., from +1° to +4°C, cells kept continuously at RT demonstrated average F_v/F_m, relative to pre-exposure levels, of +4.6, +12, +4, and −10% (CCMP421) and of +2.5, −1, −8, and −20% (CCMP2467). Reductions in F_v/F_m values due to temperature increases were not accompanied by an increase in moribund cells. Cells in strain CCMP421 still showed relatively high average F_v/F_m values after the final exposure to a temperature of +4°C (0.19 ± 0.01 at 276 min, compared to 0.30 ± 0.01 at 9 min; mean F_v/F_m ± SD; Fig. 3A), and strain CCMP2467 began to rapidly recover from its relatively low average F_v/F_m values after the final treatment (increasing from 0.03 ± 0.01 at 276 min to 0.10 ± 0.02 at 300 min; Fig. 3B). The recovery was notably different in the two strains during the 28.5-min period provided to cells immediately after being exposed to +3°C (Fig. 3, A and B, "Recovery"). From the beginning (Fig. 3, A and B, "Onset") until the end of the recovery period (Fig. 3, A and B, "End"), CCMP421 regained an average of 0.00 ± 0.01 F_v/F_m per min recovery time, whereas CCMP2467 regained 0.03 ± 0.01 F_v/F_m per min recovery time (fig. S5). The reduction and recovery of maximum photosynthetic quantum yields depended on the position of individual cells within the temperature gradient, with cells that had experienced a less extreme temperature increase showing a faster recovery (Fig. 3, A and B, bin 3) than cells that had experienced a greater temperature increase (Fig. 3, A and B, bins 1 and 2). In combination, these data suggest that CCMP2467 reacts to, and recovers from, transitory warming events more markedly than CCMP421.

Variation in the response to rising temperature between and within *Symbiodinium* strains

Beyond measuring average photophysiological parameters, PhenoChip enables measurements of single-cell properties over time and thus can relate photophysiological outcomes to prestimulus conditions on a cell-by-cell basis. Motivated by the photophysiological differences identified between the *Symbiodinium* strains, we used this capability of PhenoChip to test whether the photophysiological performance of a cell before being exposed to thermal stress could predict its ability to withstand and recover from increased temperatures, and to determine how individual cells from each population respond to progressively increasing thermal stress. To this end, for each individual cell, the F_v/F_m values from the five thermal cycles within each temperature treatment were averaged, resulting in a single average for the maximal PSII quantum yield in each temperature treatment (before temperature exposure, +1°, +2°, +3°, and +4°C). This resulted in five average F_v/F_m values to characterize the net photophysiological response of each cell upon exposure to thermal stimuli. Plotting the averaged values of single-cell F_v/F_m under elevated temperatures against the average values of F_v/F_m from before the start of the experiment ("before exposure") for each cell (Fig. 4, A and B) revealed a linear relationship between these measurements (R^2 values in Fig. 4, A and B). The initial photophysiology of a cell was thus a good predictor of its ability to withstand increased temperatures.

There was evidence for differences between the two strains in the robustness of the relationship between the initial value of F_v/F_m and the value under increased temperature. For strain CCMP421, the correlation between single-cell F_v/F_m values under elevated temperatures and F_v/F_m values from before temperature exposure was

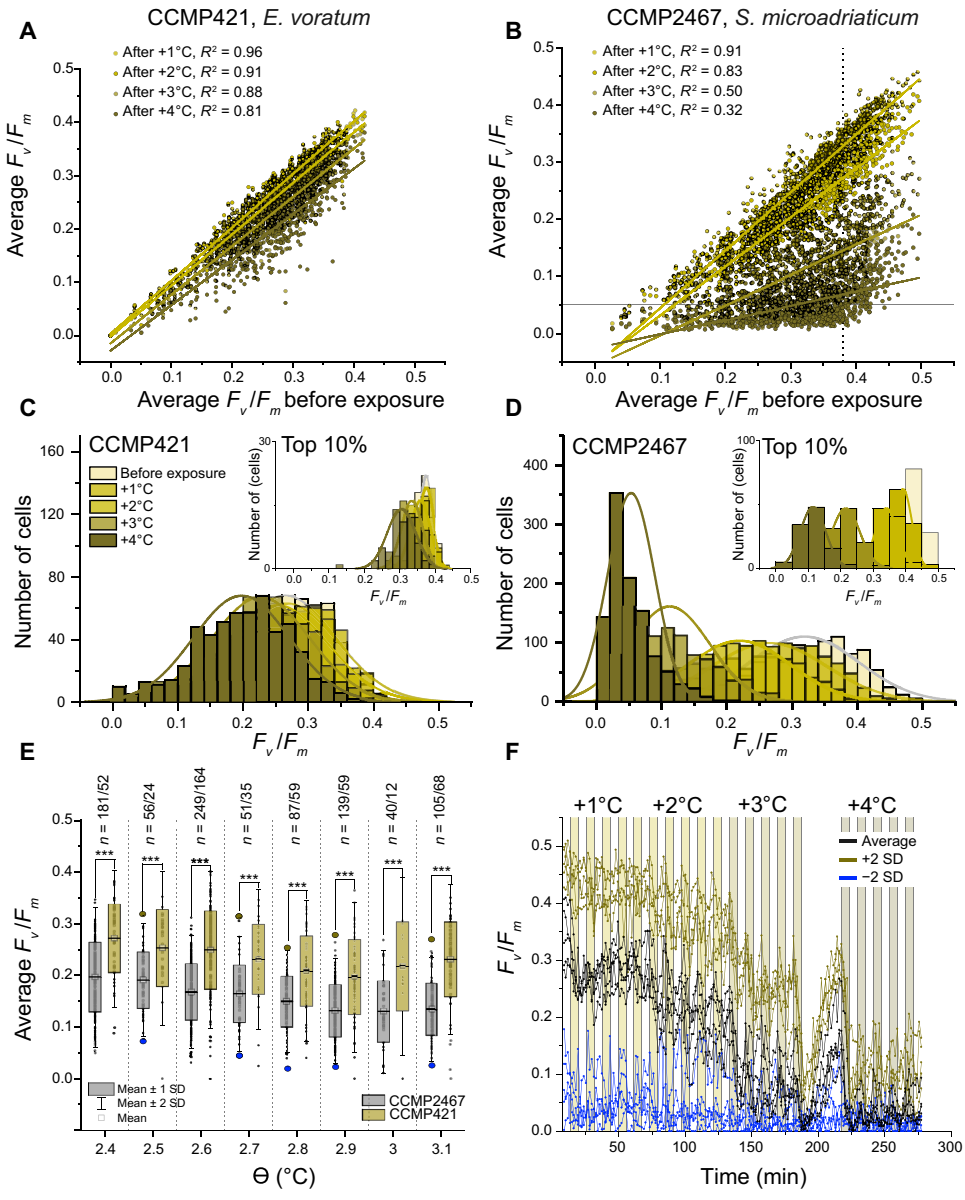

Fig. 4. Single cells of *Symbiodinium* strains CCMP421 and CCMP2467 differ in their response to elevated temperatures. (**A**) For single cells of CCMP421, the average values of F_v/F_m under each elevated temperatures (+1° to +4°C) were plotted against the average value of F_v/F_m from before temperature exposure. Linear fits of the resulting plots are shown together with their respective R^2 values (**B**) Same, for cells of CCMP2467. (**C** and **D**) Histograms of single-cell F_v/F_m values under progressively increasing temperatures in CCMP421 (C) and CCMP2467 (D). Fitting of normal distributions revealed progressively declining values of F_v/F_m in response to increasing temperatures. Insets: As in main plot, for histograms of cells with the highest F_v/F_m values before temperature exposure (top 10% of the population). Note the elevated F_v/F_m in this subpopulation compared to populations in the main panels. (**E**) Identification of temperature-resilient phenotypes by calculation of a total temperature exposure index, Θ (see the main text). Single-cell values of F_v/F_m are plotted for each temperature bin, showing the mean (white box) and 1 and 2 SDs for both strains. Asterisks indicate significant differences between the two strains (nonparametric two-sample Kolmogorov-Smirnov tests, ***$P < 0.001$). Sample sizes (n) are indicated for CCMP2467/CCMP421. (**F**) F_v/F_m under repeated thermal cycling for selected cells of CCMP2467 from (E) with mean F_v/F_m values more than 2 SDs above (brown) or below (blue) the population mean (black).

well supported and maintained for all temperature treatments ($R^2 = 0.81$ to 0.96; Fig. 4A). In contrast, for CCMP2467, the correlation was strong only for the two lower-temperature treatments (+1° and +2°C; $R^2 = 0.91$ and 0.83, respectively; Fig. 4B) and weaker for the higher-temperature treatments (+3° and +4°C; $R^2 = 0.50$ and 0.32, respectively). For CCMP2467, the weak linear correlation at higher temperatures suggested the existence of a strain-specific threshold: Cells with initial F_v/F_m values higher than the threshold maintain photosynthesis at elevated temperatures, whereas those with initial F_v/F_m values below the threshold do not. To determine this threshold, we chose a cutoff of $F_v/F_m = 0.05$ for the post-treatment value of F_v/F_m (Fig. 4B, y axis, gray horizontal line), a value corresponding to the estimated instrumentation error of the PAM imaging system. We then counted the proportion of cells that withstood the two higher-temperature treatments, defined as those above the cutoff value, at various values of initial F_v/F_m along the x axis. This analysis showed that cells with initial

F_v/F_m values greater than 0.38 (n = 264; Fig. 4B, x axis, dotted vertical line) always withstood temperature treatments of +3°C (i.e., 100% of cells, n = 264, had F_v/F_m values of >0.05 after the temperature treatment) and frequently withstood temperature treatments of +4°C (85%, n = 223). Cells from the *Symbiodinium* strain CCMP2467 thus were more sensitive toward short-term temperature perturbations than cells from strain CCMP421, and CCMP2467 exhibited a threshold for thermal tolerance of photosynthesis. Single cells from both strains were also tested for their growth under two temperatures (22° and 26°C), applied continuously for 4 days. In contrast to results from PhenoChip, single-cell growth experiments did not reveal a difference in temperature sensitivity between strains CCMP2467 and CCMP421 (fig. S6).

Individual cells within populations of *Symbiodinium* did not respond uniformly to rising temperature, rather we found subpopulations of cells that resisted temperature increases better than others. Histograms of F_v/F_m for the two strains (Fig. 4, C and D) show a normal distribution that is progressively shifted toward lower average values during each increase in temperature, with the reduction being less pronounced in strain CCMP421 (Fig. 4C) than CCMP2467 (Fig. 4D). To illustrate the heterogeneity in the response, we separately plotted the data from cells belonging to the top 10% of the population in performance before exposure to increased temperature [CCMP2467, n = 106; CCMP421, n = 58; Fig. 4, C and D (inset)]. The shift in the distribution of F_v/F_m toward lower values with rising temperature was less pronounced in this top 10% of the population than in the full population. For both strains, this result confirms our previous finding (Fig. 4, A and B) that single cells with high initial F_v/F_m generally surpassed cells with low F_v/F_m in their ability to photosynthesize during increasing temperatures.

Identification of temperature-resilient *Symbiodinium* phenotypes

The isolation of individual temperature-resilient cells would powerfully complement ongoing strategies for assisted evolution in the genus *Symbiodinium*. To allow the identification of cells with higher resilience, we formulated an index to measure the cumulative heat exposure of each single cell over the course of the entire experiment. For each applied temperature treatment, the different temperatures across the array of microwells were discretized into temperature bins with an interval of 0.25°C. From this, a total temperature exposure index (hereafter referred to as Θ) was calculated by averaging the discrete increases in temperature that each row of microwells was exposed to during all temperature treatments. The resulting index, Θ, allowed us to track the average value of F_v/F_m over all temperature treatments for each individual cell and to compare their thermal resilience to fluctuations and identify the outliers present in this subpopulation for subsequent phenotyping.

Single-cell values of F_v/F_m (Fig. 4E) for different values of Θ showed that cells from strain CCMP421 significantly outperformed cells from strain CCMP2467, with consistently higher values of F_v/F_m across all temperature exposures (Fig. 4E; nonparametric two-sample Kolmogorov-Smirnov tests $P < 0.001$ in all cases; values of n given above each boxplot). The difference between strains became more pronounced at the highest values of Θ. For example, at a value of Θ of 3.25°C, single cells of CCMP421 had a population mean $F_v/F_m = 0.26 \pm 0.05$ (n = 24), whereas single cells of CCMP2467 had a mean of 0.16 ± 0.05 (n = 30). The single-cell information provided by PhenoChip revealed a large degree of heterogeneity, i.e., a large spread around the mean, within populations of cells at each value of Θ. Further, it allowed us to identify cells that maintained significantly higher or lower F_v/F_m values compared to the population mean at each temperature treatment. To illustrate their performance, we focused on cells from the coral-associated strain CCMP2467 with values of F_v/F_m that were more than 2 SDs below (Fig. 4E, blue dots) or above (Fig. 4E, brown dots) the population mean. This resulted in a subset of cells identified from across five values of Θ (2.5°, 2.6°, 2.8°, 2.9°, and 3°C), whose F_v/F_m values we plotted across the entire experiment (Fig. 4F). This revealed that cells 2 SDs above (Fig. 4F, brown lines) the population mean (Fig. 4F, black lines) had consistently higher values of F_v/F_m throughout all temperature treatments (mean 0.46 ± 0.02 at 9 min and 0.11 ± 0.05 at 276 min, n = 5 cells) than cells 2 SDs below (Fig. 4F, blue lines) the population mean (mean 0.08 ± 0.05 at 9 min and 0.01 ± 0.01 at 276 min, n = 5 cells). These results demonstrate a large degree of single-cell phenotypic heterogeneity within two strains of *Symbiodinium*. This variability, together with the consistency of the photophysiological performance over time and throughout temperature treatments, underscores the ability of PhenoChip to identify and select individual cells with desired characteristics under specific environments from within a population.

The response of *Symbiodinium* to pH gradients

Changes in the chemical microenvironment can change the ability of phototrophs to photosynthesize. PhenoChip combined with PAM imaging allows monitoring of these changes in real time by exposing cells to a range of solute concentrations via a built-in microfluidic gradient generator (Fig. 1, A and D). Photosynthetic cells, including *Symbiodinium*, are particularly affected by pH, which can alter the efficacy of photosynthesis by shifting the availability of inorganic carbon (C_i) for photosynthesis from the less rapidly available form HCO_3^- to the more available form CO_2. We used PhenoChip to test two strains of *Symbiodinium* for their ability to photosynthesize under a range of pH values. Correct establishment of pH gradients, created by flowing solutions of pH 4.0 and 8.1 into the two inlets, was first confirmed by injecting sodium fluorescein, a compound that changes fluorescence under different protonation states (*15*), at the entry channel of the main channel (fig. S7A) and comparing the resulting fluorescence values with previously established calibration curves (fig. S7B). In this way, a pH gradient (pH 4.0 to 8.1) was established within PhenoChip and provided to single cells of *Symbiodinium* strain CCMP421 (n = 1203) or CCMP2467 (n = 2014) for 30 min. To stimulate photosynthesis in both strains, saturating photon irradiances (CCMP421, 190 μmol photons m^{-2} s^{-1}; CCMP2467, 108 μmol photons m^{-2} s^{-1}; fig. S8) were provided to cells to allow measurement of single-cell effective PSII quantum yields, Φ_{II}. All Φ_{II} measurements were performed on cells located immediately after the 10 entry channels of the main channel (fig. S7C).

The two strains differed in their response to pH. Strain CCMP421 showed significantly higher Φ_{II} than CCMP2467 at low pH (pH 4.0 to 6.0) (Fig. 5; nonparametric two-sample Kolmogorov-Smirnov tests; values of n and P values indicated above each boxplot), but similar performance at intermediate pH of 6.8 and 7.5, and lower Φ_{II} than CCMP2467 at pH 7.8. This suggests that strain CCMP2467 performs significantly better than CCMP421 at a pH range (~7.8 to 8.2) that has been estimated to occur around corals during the past 300 years (*16*).

To determine the pH at which each strain performed most efficiently, the distribution of single cell Φ_{II} was compared across pH

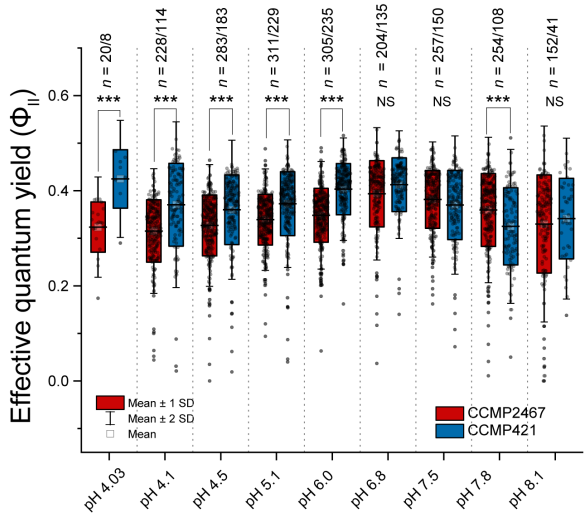

Fig. 5. *Symbiodinium* strains CCMP421 and CCMP2467 differ in their photophysiological response to pH. Plots show the effective quantum yield, Φ_{II}, at different levels of pH for single cells of *Symbiodinium* strains CCMP421 and CCMP2467 under saturating light conditions. Box and whisker plots of single-cell Φ_{II} values display the mean (white box) and 1 and 2 SDs. Differences between the two strains at each pH level were assessed using nonparametric two-sample Kolmogorov-Smirnov tests [***$P < 0.001$, and NS (not significant)]. Sample sizes (*n*) are indicated above each plot for CCMP421/CCMP2467.

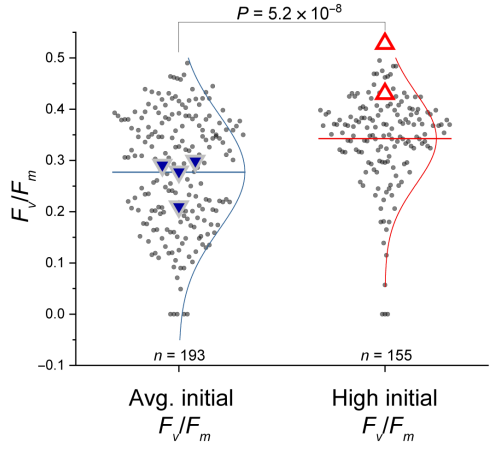

Fig. 6. Selecting and propagating single cells of *Symbiodinium* results in the transgenerational preservation of photosynthetic phenotypes. Single cells of *Symbiodinium* CCMP2467 were first assessed within PhenoChip for their maximum quantum yields, F_v/F_m, and based on this phenotypic assessment, specific photosynthetic phenotypes were ejected from PhenoChip using LCM. In this way, single cells with initial values of F_v/F_m close to the population average ($n = 4$ cells, blue triangles), and high initial values of F_v/F_m ($n = 2$ cells, red triangles) were retrieved from PhenoChip. These parent cells were propagated for 6 weeks to yield two distinct populations of cells (blue, average F_v/F_m initial population; red, high F_v/F_m initial population). The resulting populations differ in F_v/F_m ($P = 5.2 \times 10^{-8}$, nonparametric two-sample Kolmogorov-Smirnov test). Sample sizes (*n*) of single cells within propagated populations are indicated below normal distribution plots, which display the mean (blue or red line) of each population.

treatments within each strain [Kruskal-Wallis analysis of variance (ANOVA) followed by post hoc analysis, $P < 0.05$, df = 8]. For strain CCMP421, the highest population median Φ_{II} occurred at pH 6.8 (0.424, n = 135), followed by pH 6.0 (0.414, n = 235) and pH 5.1 (0.385, n = 229). Strain CCMP421 also demonstrated a high population median at a pH of 4.0 (0.43) yet with very few cells contributing to this measurement (n = 8). Significant differences were detected in 18 of 36 pairs of pH comparisons in strain CCMP421 (table S2); notably, the population medians were significantly different at pH 6.8 when tested against higher pH (7.5 to 8.1). For strain CCMP2467, the highest population median Φ_{II} occurred at a pH of 6.8 (0.41, n = 204), followed by pH 7.5 (0.39, n = 257), pH 7.8 (0.37, n = 254), and pH 8.1 (0.35, n = 152). High photosynthetic activity at pH 6.8 was confirmed in an independent single-cell Raman experiment where CCMP2467 also demonstrated the highest light-induced uptake of $H^{13}CO_3^-$ at this pH (fig. S9). In strain CCMP2467, significant differences in Φ_{II} were detected in 22 of 36 pairs of pH comparisons (table S2), and here, for example, population medians were significantly different between pH 6.8 and pH 7.8 to 8.1. Both CCMP421 and CCMP2467 thus displayed their highest photosynthetic efficiency at pH 6.8. For both strains of *Symbiodinium*, these data demonstrated a large degree of single-cell heterogeneity and photosynthetic optima in the near-physiological pH range (6.0 to 7.0).

Removal of specific individual cells from PhenoChip

To further characterize or propagate cells with specific phenotypes after their analysis within PhenoChip, it is necessary to remove them from the microwell array. The selective removal of individual cells was achieved by transferring PhenoChip onto a laser capture microdissection (LCM) platform. LCM is an optical expulsion method that relies on the application of short pulses of an ultraviolet (UV) laser to create small cavitation bubbles adjacent to specific cells within microwells. Cavitation-induced pressure changes dislodge immobilized cells (requiring an average of 1.5 attempts per cell, n = 189) and catapult them into the laminar flow stream in the main channel (movie S1), enabling their collection at the outlet of PhenoChip. As UV light is harmful to most organisms, and phototrophs in particular, we tested the effect of LCM on *Symbiodinium* strain CCMP421. Immobilized cells (n = 303) of this strain were assessed within PhenoChip for their dark-adapted maximum quantum yield (F_v/F_m). Cells (n = 189) were then expulsed using LCM and collected (resulting in successful capture of n = 161 cells; see Materials and Methods for a discussion of the loss of cells). Repeating the measurements of F_v/F_m on populations of recovered cells confirmed that the cells were not significantly affected by the expulsion procedure (nonparametric paired Wilcoxon signed rank test, $P = 0.87$, n indicated below boxplots; fig. S10). LCM can thus be used to selectively remove immobilized cells from PhenoChip without causing detectable harm to selected strains of *Symbiodinium*.

Last, we demonstrate that cells chosen within PhenoChip on the basis of their photosynthetic phenotype could be collected and propagated. Using PhenoChip, we identified and collected using LCM a small population of single CCMP2467 cells characterized by either average F_v/F_m values (0.27 ± 0.03, n = 4; Fig. 6, blue triangles) or exceptionally high F_v/F_m values (0.48 ± 0.05, n = 2; Fig. 6, red triangles). Each recovered population was propagated for 6 weeks, after which values of single-cell F_v/F_m were measured. This revealed that populations descending from cells with high F_v/F_m retained significantly higher values of F_v/F_m than populations propagated from cells with average F_v/F_m values [Fig. 6; 0.34 ± 0.08, n = 155 (red distribution) and 0.28 ± 0.11, n = 193 (blue distribution), respectively; nonparametric two-sample Kolmogorov-Smirnov test, $P = 5.2 \times 10^{-8}$]. These data

demonstrate that specific cells can be isolated and propagated from PhenoChip and that photosynthetic phenotypes are preserved in *Symbiodinium* CCMP2467 after 6 weeks of culture (corresponding to approximately 14 to 17 generations).

DISCUSSION

The development of microfluidics has revolutionized our ability to phenotype single cells for desirable traits. Single cells can now be examined in microdroplets (*17*), on capture pads (*18*), or in large-scale microwell arrays (*19*) by a multitude of biochemical or biophysical interrogation methods (*20*). Owing to its impact, the use of microfluidic-assisted single-cell phenotyping is now not only becoming more customary in multiple disciplines, from oncology to antimicrobial susceptibility testing, but is also used for the phenotyping and assessment of nonclinical organisms such as microalgae (*13*). While these technologies provide rich details on the population heterogeneity of phenotypes, they often lack the ability to provide measurements of the same individual cell over time and in response to environmental stress. PhenoChip allows the application of multimodal environmental perturbations to an array of individually immobilized photosynthetic cells in combination with the observation of their photophysiology at the single-cell level in near real time. While conceptually similar to large-scale plant phenotyping platforms, the miniaturized dimensions of PhenoChip now enable high-throughput phenotyping of single microalgae and cyanobacteria based on their photosynthetic performance.

To achieve this, we combined PhenoChip with PAM, a variable chlorophyll fluorescence technique that quantifies an array of photophysiologically important parameters at a high spatiotemporal resolution (*21*). The provision of relevant environments in phenotyping efforts has been shown to be crucial in detecting the emergence of phenotypes capable of coping with environmental stress (*1*). In contrast to most other comparable microfluidic phenotyping platforms (*13*), PhenoChip is therefore equipped to expose single phototrophic cells to dynamic environmental conditions such as spatiotemporal gradients of temperature (*3*) and pH. PhenoChip permits the continuous interrogation of the same single cells under environmental perturbations, which is advantageous for their phenotyping, but correspondingly results in a lower throughput when compared to typical droplet-based phenotyping screens. When compared with other continuous observation platforms, e.g., single-cell microrespirometry (*19*) or bacterial "mother-machines" (*22*), PhenoChip can reach similar high-throughput assessment rates and monitor the same 500 to 1000 cells repeatedly. We have here illustrated the power of PhenoChip to uncover heterogeneity within populations and its potential for precise phenotyping and selection of microorganisms, using the example of short-term environmental stress tolerance in the microalga *Symbiodinium*.

Because of its fundamental role in coral health, *Symbiodinium* has been extensively studied for its thermal sensitivity in cultures and in hospite. This research has revealed that *Symbiodinium* phylotypes ("clades") (*23*) can vary in their temperature sensitivity as a result of, for example, differences in PSII repair efficiency (*14*) or susceptibility of PSII to photobleaching (*24*). Yet, despite the systematic investigation in bulk cultures, little is known about the single-cell variability within or between clades, knowledge that, in other microbial systems, has uncovered the presence of high levels of phenotypic heterogeneity even under static conditions and in clonal populations (*25*). In the context of phenotyping, this heterogeneity is particularly important, as it might permit certain genotypes within a population to better resist environmental fluctuations (*12*) and could provide a basis for their selection via assisted evolution approaches. Phenotyping of cells using PhenoChip revealed differences in the response to transiently applied temperature increases in the two strains of *Symbiodinium*, CCMP2467 [clade A1, *S. microadriaticum* (*6*)] and CCMP421 [clade E, *E. voratum* (*6*)]. Under moderate thermal stress, they demonstrated distinguishable patterns of stress-induced effects on PSII or other energy dissipation mechanisms: The symbiotic strain CCMP2467 was characterized by a generally higher sensitivity and faster recovery in F_v/F_m than the nonsymbiotic, free-living strain CCMP421. Besides the inactivation of PSII, other energy dissipation mechanisms, however, will likely also contribute to the reduction of F_v/F_m, particularly the state of the primary electron acceptor quinone molecule (Q_A), nonphotochemical quenching (NPQ) pathways, and changes in the light harvesting antenna system of *Symbiodinium* that could potentially be affected by the repeated probing of photosynthesis in conjunction with temperature perturbations.

Exposure of strain CCMP2467 to progressively increasing temperatures revealed a thermal sensitivity threshold in the prestress value of F_v/F_m. Cells with initial values of F_v/F_m above 0.38 effectively maintained photosynthesis for temperature increases as high as +4°C, whereas cells with initial values of F_v/F_m below the threshold of 0.38 became severely impaired under these temperature increases. Under identical experimental conditions, no thermal sensitivity threshold was evident in strain CCMP421. Four-day-long observations of single-cell growth at 22° or 26°C did not suggest that strain CCMP2467 is less temperature resilient than CCMP421, however (fig. S6). We hypothesize that these opposing observations are a result of the time scales at which temperature perturbations were applied: Within PhenoChip, temperatures were transiently applied to cells, allowing no time for acclimation, while cells in growth experiments experienced continuous temperatures, permitting them to acclimate. These results underscore the importance of a device like PhenoChip, which allows probing of the effects of environmental perturbations on single-cell photosynthetic phenotypes across a continuum of spatiotemporal time scales. Together, these data thus support the existence of varying temperature sensitivities between clades (*26*) and thermal sensitivity thresholds across time scales in some clades but not others. Whether these thermal sensitivity thresholds from laboratory cultivars are useful in forecasting bleaching events within coral holobionts remains, for now, speculative. To examine this further, we intend to use PhenoChip to survey the thermal sensitivity of native *Symbiodinium* cells isolated from corals in the field and to compare this with endosymbiotic cells in hospite within coral holobionts.

We found evidence for high single-cell variability in photosynthetic responses in both *Symbiodinium* strains and the existence of subpopulations of cells that maintained photosynthesis under high temperatures. Earlier studies that investigated single *Symbiodinium* cells, inside and outside of corals, also found variability in F_v/F_m (*27*, *28*), suggesting that population variability goes unrecognized when traditional bulk methods are used. While the source of this variability is unknown, our data demonstrate that individual cells with high initial F_v/F_m values consistently outperformed cells with lower initial F_v/F_m values during elevated temperatures. Because of this consistency in response, these cells would provide a promising target for efforts to select cells that are tolerant to thermal stress.

Consequently, we targeted single *Symbiodinium* phenotypes with high F_v/F_m in a proof-of-concept selection and propagation effort. Selecting and propagating single *Symbiodinium* cells with values of F_v/F_m above average resulted in bulk populations that maintained higher than average F_v/F_m values after 6 weeks of growth under stable environmental conditions. It was not determined whether these bulk populations of *Symbiodinium* consisted of a specific cell that outgrew others and dominated the resulting populations. Whether cells in bulk populations are permanently imbued with elevated resilience toward temperature increases will be tested in a follow-up study. Together, these efforts indicate that, by providing a means to manipulate conditions, assay, and select individual cells, PhenoChip will provide a valuable tool in assisted evolution of photosynthetic cells under strong environmental selective forces.

Coral reefs are also threatened by ocean acidification, which directly affects photosynthetic organisms by shifting the availability of C_i from HCO_3^- to CO_2, and for reefs specifically, by weakening their ability to deposit calcium carbonate (*8*). However, cells of *Symbiodinium* are also adapted to very low pH; recent studies have shown that the coral host acidifies the compartment (the "symbiosome") around endosymbionts to a pH of approximately 4, which provides the most photosynthetically accessible form of C_i (CO_2) to *Symbiodinium* (*29*). Within PhenoChip, our expectation was thus that *Symbiodinium* cells exposed to pH < 6.0 would show increased carbon fixation and thereby increased effective quantum yields (Φ_{II}), as previously reported in filamentous green algae (*30*). Instead, in both strains, we found the highest Φ_{II} to occur at pH 6.8. This pH optimum for Φ_{II} was additionally confirmed by initial experiments combining PhenoChip with single-cell Raman microspectroscopy, which, for single cells of *Symbiodinium* CCMP2467, revealed the strongest $H^{13}CO_3^-$ uptake to also occur at a pH of 6.8 (described in fig. S9). This corroborated our PAM-derived findings and emphasized the ability of PhenoChip to uncover single-cell metabolic heterogeneities using other imaging modalities. The effect of variation in pH on population averages of Φ_{II} was generally small in both strains and so was the effect of pH on the variability of single-cell Φ_{II}. This suggests that single cells from the two laboratory strains of *Symbiodinium* can effectively access both forms of C_i and maintain cytoplasmic homeostasis in the face of large external pH shifts during the relatively short time scales of our experiments (~30 min), not unlike other algae (*31*). On the transcriptome level, *Symbiodinium* down-regulates carbon acquisition/fixation upon exposure to a reduction in pH lasting 3 hours (*32*), which suggests that longer pH exposure could result in more pronounced effects on photosynthesis. In this context, PhenoChip has already been successfully used with *Symbiodinium* for 7 days, a time frame that would enable investigation of the effects of longer-term chemical (or temperature) exposure and, ultimately, enable the selection and propagation of phenotypes capable of tolerating, for example, projected conditions of ocean acidification or toxins relevant to coral health such as sunscreens.

It has been suggested that developing coral stocks with enhanced stress tolerance could help alleviate the threat to coral reefs from projected changes in sea surface temperatures (*10*). Current mitigation strategies include the rearing of *Symbiodinium* cultures under thermal stress (*11*), the investigation of coral microbiomes (*33*), and other assisted evolution approaches (*10*), along with studies of corals apparently thriving under extreme environmental conditions (*34*). PhenoChip could augment these mitigation strategies by adding the critical resolution required to assess *Symbiodinium* and select single-cell phenotypes under environmental conditions to start elucidating the molecular and physiological basis of their thermal and chemical resilience. First proof-of-concept data highlight PhenoChip's versatility in assessing phototrophic responses under relevant environmental perturbations and its promise in opening the door to high-resolution and high-throughput phenotyping of cells for biotechnology and unified testing of chemical and environmental hazards in ecotoxicology.

MATERIALS AND METHODS

Additional information on how to avoid common problems during the operation of PhenoChip is included in Supplementary Materials.

Microfluidic device construction

PhenoChip was constructed using standard photolithography techniques in clean-room facilities. Silicon wafers were used as a substrate and baked for 2 hours at 200°C to remove residual moisture before negative SU-8 photoresist (SU8-3050, MicroChem Corp., Newton MA) was spin-coated at ~2500 rpm for 45 s for the first layer deposition (~75 μm). The silicon wafer was baked for 10 min to remove residual solvent, cooled to RT, and then exposed to 250 mJ cm^2 UV using multiple exposure modes on a mask aligner (Karl Suss MA6, SUSS MicroTec SE, Garching, Germany) through a high-resolution plastic photomask (Micro Lithography Services Limited, Chelmsford, UK). Wafers were postexposure baked at 65°C for 1 min and at 95°C for 5 min to cross-link UV-exposed areas and then slowly cooled back to RT (T = 22°C). Wafers bearing the first layer were used as substrate in a second layer deposition. Using a similar protocol but with a different photoresist (SU8-3010), spin-coating speed (1000 rpm), a new photomask, and altered baking times per manufacturer recommendations, a second layer of ~15 μm was deposited to create the microwell array (57 rows × 511 columns = 29,127 wells, filling the entire main channel area). After a second postexposure bake (65°C for 1 min and 95°C for 3 min), the resulting wafer was immersed in SU-8 developer (mr-Dev 600, MicroChem Corp.) to remove noncross-linked photoresist and then repeatedly washed with fresh developer and isopropanol. Features were visually inspected using an upright reflected light illumination microscope (Nikon Eclipse L200, Nikon Corp., Tokyo, Japan) equipped with a 40× objective, and their heights were measured using a surface profilometer (Dektak Stylus Profiler, Bruker, Billerica, MA, USA). Actual heights were 75 μm for the primary layer and 12.5 μm for the secondary (microwell) layer. The final wafers (= master molds) were placed in a vacuum desiccator, and (tridecafluoro-1,1,2,2-tetrahydrooctyl)-1-trichlorosilane was deposited on the exposed silica surface to aid in the detachment of the microfluidic device after curing.

Master molds were used as a substrate for poly(dimethylsiloxane) (PDMS) replica molding. PDMS was mixed with its cross-linker at a 10:1 (w/v) ratio and poured onto the master mold, which was placed in a desiccator chamber and degassed for ~15 min. Residual bubbles were removed using compressed air, and the PDMS was cured overnight at 80°C. Cured PDMS was manually removed from the master with a scalpel, and individual PhenoChips were cut to fit on a standard microscopy slide (25 mm by 75 mm). PDMS surfaces were covered in Scotch tape, and inlet and outlet holes were created using a biopsy puncher (1.5 mm in diameter, World Precision Instruments, Sarasota, FL, USA). PhenoChips were then bonded to isopropanol-cleaned microscopy slides using O_2 plasma (Zepto 1, Diener electronics GmbH,

Ebhausen, Germany) applied for a duration of 1 min at 50% maximal intensity. Bonding was finalized by placing PhenoChips on an 80°C hotplate for >3 hours. Devices were kept covered in Scotch tape in a Petri dish until use. Computer-aided design files for PhenoChip are found as a supplementary file in the online version of this manuscript.

Cell culture conditions

Symbiodinium strains CCMP421 (= *E. voratum*) and CCMP2467 (= *S. microadriaticum*) were obtained from the Bigelow culture collection. These cultures were nonaxenic, and no antimicrobial control agents were added during experiments or standard maintenance. Cultures were maintained in f/2 medium prepared from autoclaved and sterile-filtered artificial saltwater (Instant Ocean, Aquarium Systems, Sarrebourg, France) at a salinity of 33 to 36 (parts per thousand) and a pH of 8.0. Cells were grown in Nunclon EasYFlasks with a volume of 25 cm^3 (Thermo Fisher Scientific, Waltham, MA, USA) without shaking and ample headspace for gas exchange. The temperature was maintained at 23°C, and irradiance was provided by white light-emitting diodes (LEDs), providing a photon irradiance (400 to 700 nm) at ~100 μmol photons m^{-2} s^{-1} over a 14-hour/10-hour day/night cycle. Irradiance was quantified in cultivation vessels filled with medium using a ULM-500 light meter (Walz, Effeltrich, Germany) equipped with a calibrated, submersible spherical quantum sensor (3-mm tip diameter, US-SQS/L, Walz). Two weeks before experiments, cells were inoculated in fresh f/2 medium at a 1:100 (v/v) dilution, resulting in midexponentially growing cultures on the days of the experiments. All experiments with *Symbiodinium* were started 6 hours after the onset of the day cycle and lasted <5 hours to avoid life stage transitions (e.g., from nonmotile to motile) that typically occur 2.5 to 4 hours after subjective dawn.

Cell loading

To allow complete liquid filling of the microwell array, PhenoChips were placed in a vacuum for 10 to 15 min, followed by immediate injection of sterile f/2 medium. Omission of the vacuum step caused a number of wells to be air filled. Before loading, *Symbiodinium* cells (~6 to 8 ml) were mixed thoroughly by shaking the cultivation vessel and then centrifuged for 2 min at 1500 relative centrifugal force (rcf), the supernatant removed, and the cells were resuspended in ~100-μl f/2 medium. The resulting highly concentrated cell suspension was injected into the outlet of the PhenoChip until the microwell array was overlaid with cells. Cells were then loaded into wells by compressing the flexible PDMS main channel, which impressed cells into wells. Compression was achieved by gently placing the blunt end of a pair of forceps onto the main channel and slowly moving it across the main channel from inlet to outlet. This procedure lasted approximately 20 s. After this procedure, the remaining nonimmobilized cells were washed out of the main channel by flushing with a pipette. No further compression was applied for the remainder of the experiment, and cells were left in the open confinement of microwells hereafter.

This procedure caused no significant difference in F_v/F_m between unrestricted and immobilized populations ($P = 0.10$, nonparametric two-sample Kolmogorov-Smirnov test; fig. S1). The effectiveness of the loading procedure was found to depend principally on (i) cell dimensions, which can vary, e.g., among different growth stages of unicells; and (ii) well size, which can be tuned during device fabrication. We have successfully used PhenoChip to immobilize cells of varying sizes into microwells; i.e., *Symbiodinium* (10 to 12 μm in diameter in this study), unicellular cyanobacteria (*Prochloron* spp.; diameter, 5 to 25 μm), and red algae (*Galdieria* spp.; diameter, 5 to 10 μm). For *Symbiodinium*, in particular, we found that a well size of 20 μm was sufficient to accommodate all cell sizes within its life-cycle. The application of PhenoChip to other phototrophic cells requires verification that cells (i) remain immobilized within existing geometries for the desired experimental time frame; (ii) are unharmed by the loading procedure; (iii) emit enough signal for chlorophyll fluorometry (see below); and, if retrieval of cells is necessary, (iv) that cells can be removed using optical expulsion techniques (see below). It is important, for the use of PhenoChip, to ensure that the organism of choice is compatible with PAM-based variable chlorophyll fluorescence imaging. PAM measurements on certain cyanobacteria are, e.g., affected by nonvariable background fluorescence from phycobilisomes, the redox state of the plastoquinone pool, or respiratory electron flow in thylakoid membranes, and state transitions between PSII and PSI can occur in cyanobacteria and green algae, even under darkness. For *Symbiodinium,* a well diameter of 20 μm yielded a good compromise between loading efficiency (~40% of wells were routinely filled), multiple cell occupancies (~65% of occupied wells), and loss rate (1.4 to 4.2% of cell populations lost during a 4.5-hour experiment). To obtain higher loading efficiency, double occupancies were accepted, and the identification of single cells was performed during postprocessing using standard image analysis tools (see below).

Temperature oscillations

Large side channels (length, 24.5 mm; width, 2.5 mm) within PhenoChip were filled with a silver-laced epoxy polymer (Epo-Tek H20S, Epoxy Technology Inc., Billerica, MA, USA) as previously used in microfluidic devices (*3*). This conductive path length was found to be sufficiently long to create homogeneous temperature gradients across the microwell arena. Because of the high viscosity of the polymer and the associated slow filling, compressed air was used to accelerate the injection of the epoxy and to create some overflow of the material in both the inlet and outlet of the channel. Small (1 mm in diameter) copper cables were inserted into the inlet and outlet, and the chip was left to cure at 80°C on a hotplate for 2 hours. Chips were tested for electrical conductivity using a DC power supply (RND 320-KD3005D, Distrelec group AG, Nänikon, Switzerland), and a temperature-sensitive liquid crystal (LC) sheet of appropriate temperature range (20° to 25° and 25° to 30°C; Edmund Optics, Barrington, NJ, USA) was placed onto the device. This permitted a rapid assessment of obvious heterogeneities in temperature gradients, which can occasionally occur at the connection wires (*3*), and allowed the most homogeneous devices to be chosen for subsequent calibration. Calibration of temperature gradients was achieved by first exposing LC sheets mounted on a microscope slide to known temperatures using a flow-through water bath (F32, JULABO GmbH, Seelbach, Germany) attached to a custom-made aluminum flow-through cell. The colorimetric changes occurring at specific temperatures were recorded using an RGB (red, green, and blue) camera (Canon EOS 6D, Canon Corp., Japan) under a homogeneous illumination field provided by a NeoPixel RGB LED 15 ring (Adafruit Corp., New York City, NY, USA), both attached to a dissecting scope (Nikon SMZ-U, Nikon Corp., Tokyo, Japan). Images were analyzed in Fiji (https://imagej.net/Fiji), and the intensity of the blue channel was found to follow a linear relationship with temperature. The same LC sheets were then used with PhenoChips to select the combinations of voltage and current to achieve the desired

temperature gradients. The relation between input current and resulting temperature was linear (adjusted R^2 = 0.94; fig. S3), with a temperature increase of approximately +1°C above RT (measured in the middle of the main channel at constant flow) for each 2.5 mA increase in current (fig. S3). Confirmation of the resulting temperatures was obtained using a type K thermocouple thermometer with an accuracy of ±0.05% (Fluke 52II, Fluke, Everett, WA, USA), and measurements were performed with the probe fixed in the middle of the main channel, the source, or the sink. CFD modeling confirmed the linear nature of the thermal gradients and permitted the estimation of temperatures experienced by cells within the 57 rows of microwells in PhenoChip under progressively increasing temperatures (Fig. 2, A and B, and table S1). Because of the non-instantaneous nature of heat transport within multimaterial (glass, PDMS, and water) microfluidic devices, additional CFD modeling and time-lapse videography were used to obtain information about the time scale of heating and cooling, which demonstrated that steady-state temperatures (here defined as less than 0.05% temperature change) were established within ~300 s of heating or cooling (Fig. 2C).

Solute gradients

Solute mixing and delivery to cells was achieved using a Christmas tree gradient generator positioned before the microwell array (Fig. 1, A and D). To provide nonpulsatile fluid motion, low-friction 25-ml glass syringes (Hamilton 1000 series, Hamilton Corp., Reno, NV, USA) were used in conjunction with a Cetoni neMESYS syringe pump (Cetoni GmbH, Korbussen, Germany). All experiments were performed using a flow rate of 400 µl hour^{-1} injected into each inlet, a flow rate which was experimentally determined to not cause adverse effects via, e.g., shear stress (fig. S2). The accuracy of the mixing platform was tested by injecting deionized water augmented with sodium fluorescein at a concentration of 10 µM into one of the inlets and deionized water into the other. The resultant concentration profiles of sodium fluorescein were recorded using an Axio Scope A1 upright fluorescence microscope (Carl Zeiss, Jena, Germany) equipped with a Lumencor SOLA Light engine (Lumencor Inc., Beaverton, OR, USA) and a green fluorescent protein–specific fluorescence cube (Carl Zeiss, Jena, Germany). The resulting fluorescence intensities were used to validate a CFD model (fig. S7C). Direct calibration of pH gradients was possible by taking advantage of the pH-dependent changes in fluorescence emission of sodium fluorescein (*15*). For calibration, f/2 media with 10 µM sodium fluorescein and known pH (pH 4.0, 5.1, 5.9, 7.2, 8.1, and 9.0, measured and titrated to the desired pH on a FiveEasy Plus pH meter; Mettler Toledo, Columbus, OH, USA) were injected into the PhenoChip, and the resultant fluorescence was recorded at the entry channels of the microfluidic gradient generator into the main channel (fig. S7A). Between measurements at each level of pH, the chip was washed with deionized water until the fluorescence reverted to background values. This procedure yielded a pH calibration curve (fig. S7B). For experiments with *Symbiodinium*, gradients of pH were generated by injecting f/2 medium solutions of pH 4.0 and pH 8.1 (each containing 10 µM sodium fluorescein) into the two separate inlets. The resulting fluorescence gradients were used to calculate local pH concentrations based on the calibration curve. Using this approach, pH gradients (pH 4.0 to 8.1) could be generated within PhenoChip. All pH experiments used data from cells located directly after the entry channels of the microfluidic gradient generator (fig. S7a).

CFD modeling

Heat and mass transfer and fluid flow in the microfluidic device were modeled by solving the continuity, momentum, diffusion, and energy equations for both the solid (heat) and fluid (heat, mass, and momentum) subdomains using COMSOL Multiphysics 5.3 (COMSOL). For the temperature gradients, the fluid flow and heat transfer were solved under laminar unsteady-state conditions, with no-slip boundary conditions at the microchannel walls. The following parameters were imposed in the numerical simulation: average velocity at the inlet of the middle channel, 0.0013 m s^{-1}; pressure at the outlet of the middle channel, 0 Pa. An unsteady-state heat flux was set at the walls of the source channel. A convective heat flux condition with heat transfer coefficient h = 1000 W/(m^2·K) and temperature T = 22°C was set at the sink channel. A convective heat flux condition with h = 10 W/(m^2·K) and T = 22°C was set at the external walls of the microfluidic device, simulating the natural convection at external boundaries exposed to air at RT. For the modeling of chemical gradients, fluid in the device was assumed to behave as a constant incompressible fluid (water at RT), and the incompressible continuity and Navier-Stokes equations as well as the diffusion equation were solved for fluid flow and concentration analysis. Fluid flow was assumed laminar under steady-state conditions, with no-slip boundary conditions at the microchannel walls. The numerical simulation used the following parameters: average velocity at both inlets, 0.0074 m s^{-1}; pressure at the outlet, 0 Pa; inlet concentrations, 0.01 and 0 mol m^{-3}; diffusion coefficient, 5×10^{-10} m^2 s^{-1}.

PAM imaging

A multicolor variable chlorophyll fluorescence imaging microscope (IMAG-RGB; Heinz Walz GmbH, Effeltrich, Germany) was used to quantify the photosynthetic activity of individual cells. For *Symbiodinium*, visualization with a 10× objective (Zeiss Fluar 10×/ 0.5) was sufficient to obtain accurate fluorescence readouts with ~500 to 1500 cells per field of view, without noticeable drift in XYZ during experiments. A detailed technical description of the microscope system can be found elsewhere (*35*). Using the saturation pulse method (*21*), which is based on recording fluorescence yields before and during a saturating light pulse, the maximum quantum yield of photosynthetic energy conversion in PSII, $F_v/F_m = (F_m - F_0)/F_m$, was measured after cells were given an initial 15-min dark period. The effective PSII quantum yield, $\Phi_{II} = (F_{m'} - F)/F_{m'}$, was measured at saturating photon irradiances (defined below). Here, F_v, F_m, and F_0 define the variable, maximal, and minimal fluorescence of dark-adapted cells, respectively; F is the fluorescence emission from dark-adapted cells, and $F_{m'}$ is the maximal fluorescence of light-adapted cells. For a full overview of the chlorophyll fluorescence parameters used, we guide the reader to a comprehensive review (*21*). Dark-adapted maximum quantum yields, F_v/F_m, without continuous saturation probing was measured in determining the cell viability before and after LCM (fig. S10) and before and after cell immobilization (fig. S1). To determine the photophysiological effects of short-term temperature perturbations, maximum quantum yields, F_v/F_m, were determined in darkness at an acquisition frequency of 90 s between saturating probing light pulses for all temperature experiments (Figs. 3 and 4 and fig. S5) and during cell extractions (Fig. 6). This measurement interval apparently leads to incomplete dissipation of NPQ, altered redox states of the Q_A, and possibly other changes in the light harvesting antenna system of *Symbiodinium* (*36*). Consequently, this acquisition frequency caused a reduction of F_v/F_m by ~25% relative

to the initial dark-adapted state, F_v/F_m (fig. S4). All temperature and extraction experiments were started after cells had reached steady-state values of F_v/F_m, immediately after the 10th saturation pulse (>900 s into the experiment).

For pH experiments, Φ_{II} was determined after cells had been incubated for 30 min with pH gradients and saturating photon irradiances previously determined for each strain (defined below). Photosynthetically active radiation (PAR; 400 to 700 nm) was provided by RGB LEDs, which were calibrated before each experiment using a quantum sensor (MC-MQS, Walz, Effeltrich, Germany) connected to a light meter (ULM-500, Walz). To determine the saturating photon irradiances for both strains, rapid light curves (relative electron transport rates, rETR, versus photon irradiance) were established using previously dark-adapted cells, which resulted in saturating photon irradiances of 108 µmol photons m^{-2} s^{-1} for strain CCMP2467 and 190 µmol photons m^{-2} s^{-1} for strain CCMP421 (fig. S8). Relative rates of PSII-driven electron transport were calculated using the system software as rETR = PAR × Φ_{II}.

Chlorophyll fluorescence images were captured using the supplied ImagingWin PAM software (Walz GmbH, Germany). The ImagingWin software enables correction for heterogeneities in the measuring beam, based on acquired fluorescence images with a homogeneous fluorescence standard in conjunction with a built-in background normalization of subsequent experimental images. Correct background normalization was manually inspected by comparing areas of interest on the outer edges of the images against those in the middle of the image. To prevent incorrect estimates of photosynthetic efficiencies, areas of heterogeneous actinic illumination, as previously identified via the fluorescence standard measurements, were excluded from all subsequent image analysis. In our PAM system, this resulted in the exclusion of the leftmost five columns of microwells from all images. After experiments, light transmission images were combined with PAM-derived image stacks within Fiji and registered to avoid artifacts arising from XY shifts. Single cells were manually identified within the light transmission image, and the resulting mask was used to quantify F_v/F_m and Φ_{II} from chlorophyll fluorescence images using an in-house Fiji script.

Laser capture microdissection

To test the ability to collect single cells from within PhenoChip after their phenotyping and confirm that they were not harmed by the process, cells of *Symbiodinium* CCMP421 were immobilized in microwells, and their maximum photosynthetic quantum yield, F_v/F_m, was measured in fully (15 min) dark-adapted cells (n = 303). The position of microwells was then used to identify the same cells on a laser microdissection platform (PALM MicroBeam, Carl Zeiss, Jena, Germany). Using this platform, individual cells were removed from microwells by applying a short (~200 ns) pulse of 355-nm laser light to the PDMS wall adjacent to the cell (distance, ~10 µm), always downstream of the flow direction. This resulted in the visible formation of a cavitation bubble (see movie S1), which dislodged immobilized cells (requiring an average of 1.5 attempts per cell, n = 189) and catapulted them into the laminar flow of f/2 medium supplied at a rate of 400 µl $hour^{-1}$ in each inlet. During selection, particular care was taken to avoid introduction of undesired cells into the pool of selected cells. This involved (i) extensively and repeatedly washing the main channel before selection procedures to wash away nonimmobilized cells; (ii) repeatedly tapping PhenoChip with the blunt end of a pair of forceps after cell immobilization until cells no longer entered the flow stream (checked by microscopy); if possible, (iii) selecting cells close to the outlet to reduce the potential for contamination; and (iv) exchanging the tubing before each selection process. Ejected cells (n = 189) were collected downstream and pooled in a 2-ml Eppendorf vial. After centrifuging the vial at 1500 rcf for 2 min to remove the supernatant, cells were placed onto microscopy slides with a sealing gasket (height, 500 µm), covered with a coverslip and fully dark-adapted for 15 min before performing a single measurement of F_v/F_m. Using this procedure, 161 cells could be recovered. Cells unaccounted for (n = 28) were likely lost during supernatant removal or cell adhesion within tubing from the outlet.

To demonstrate the use of PhenoChip to isolate specific cells for culture based on their phenotype, *Symbiodinium* CCMP2467 cells were immobilized and measured within PhenoChip for their maximum photosynthetic quantum yield, F_v/F_m, every 90 s for 30 min in previously dark-adapted cells (n = 70). Resulting F_v/F_m values were used to identify cells for subsequent ejection using LCM. For propagation, ejected cells were captured in sterile 2-ml low-absorption spectrometry vials (Supelco, Bellefonte, PA, USA) filled with 1.5-ml fresh f/2 medium with a salinity of 33 ppt and a pH of 8.0. Glass vials were incubated for 6 weeks at a temperature of 23°C, and irradiance was provided by white LEDs, providing a photon irradiance (400 to 700 nm) at ~100 µmol photons m^{-2} s^{-1} over a 14-hour/10-hour day/night cycle. This incubation period corresponded to approximately 14 to 17 generations in *Symbiodinium* CCMP2467. After this period, cells were carefully pipetted from the glass vials and centrifuged in 2-ml Eppendorf vials at 1500 rcf for 2 min to remove the supernatant. Cells were then pooled and placed onto microscopy slides with a sealing gasket (height, 500 µm), and their F_v/F_m values were measured every 90 s for 30 min in previously dark-adapted cells.

Statistical analysis

Data were analyzed using OriginPro 2018 (b9.5.0.193, OriginLab Corporation, Northampton, MA, USA). The significance level for all tests was set at 0.05. Linear correlations were performed using the "simple fit" application within Origin, and adjusted R^2 values are displayed. Comparisons were performed using two-sample nonparametric Kolmogorov Smirnov testing, nonparametric paired Wilcoxon signed rank testing, or Kruskal-Wallis ANOVA, followed by post hoc testing via the "Post hoc Analysis for Nonparametric Tests" application.

SUPPLEMENTARY MATERIALS

Supplementary material for this article is available at http://advances.sciencemag.org/cgi/content/full/6/36/eabb2754/DC1

View/request a protocol for this paper from *Bio-protocol*.

REFERENCES AND NOTES

1. J. A. Cruz, L. J. Savage, R. Zegarac, C. C. Hall, M. Satoh-Cruz, G. A. Davis, W. K. Kovac, J. Chen, D. M. Kramer, Dynamic environmental photosynthetic imaging reveals emergent phenotypes. *Cell Syst.* **2**, 365–377 (2016).
2. E. Litchman, K. Edwards, C. Klausmeier, M. Thomas, Phytoplankton niches, traits and eco-evolutionary responses to global environmental change. *Mar. Ecol. Prog. Ser.* **470**, 235–248 (2012).
3. D. Vigolo, R. Rusconi, R. Piazza, H. A. Stone, A portable device for temperature control along microchannels. *Lab Chip* **10**, 795 (2010).
4. H. S. Kim, T. P. Devarenne, A. Han, A high-throughput microfluidic single-cell screening platform capable of selective cell extraction. *Lab Chip* **15**, 2467–2475 (2015).
5. C. S. Luke, J. Selimkhanov, L. Baumgart, S. E. Cohen, S. S. Golden, N. A. Cookson, J. Hasty, A microfluidic platform for long-term monitoring of algae in a dynamic environment. *ACS Synth. Biol.* **5**, 8–14 (2016).

6. T. C. Lajeunesse, J. E. Parkinson, P. W. Gabrielson, H. J. Jeong, J. D. Reimer, C. R. Voolstra, S. R. Santos, Systematic revision of Symbiodiniaceae highlights the antiquity and diversity of coral endosymbionts. *Curr. Biol.* **28**, 2570–2580.e6 (2018).
7. J. M. Pandolfi, S. R. Connolly, D. J. Marshall, A. L. Cohen, Projecting coral reef futures under global warming and ocean acidification. *Science* **333**, 418–422 (2011).
8. R. Albright, L. Caldeira, J. Hosfelt, L. Kwiatkowski, J. K. Maclaren, B. M. Mason, Y. Nebuchina, A. Ninokawa, J. Pongratz, K. L. Ricke, T. Rivlin, K. Schneider, M. Sesboüé, K. Shamberger, J. Silverman, K. Wolfe, K. Zhu, K. Caldeira, Reversal of ocean acidification enhances net coral reef calcification. *Nature* **531**, 362–365 (2016).
9. V. Cumbo, M. van Oppen, A. Baird, Temperature and *Symbiodinium* physiology affect the establishment and development of symbiosis in corals. *Mar. Ecol. Prog. Ser.* **587**, 117–127 (2018).
10. M. J. H. van Oppen, J. K. Oliver, H. M. Putnam, R. D. Gates, Building coral reef resilience through assisted evolution. *Proc. Natl. Acad. Sci. U.S.A.* **112**, 2307–2313 (2015).
11. L. J. Chakravarti, M. J. H. van Oppen, Experimental evolution in coral photosymbionts as a tool to increase thermal tolerance. *Front. Mar. Sci.* **5**, 227 (2018).
12. M. Ackermann, A functional perspective on phenotypic heterogeneity in microorganisms. *Nat. Rev. Microbiol.* **13**, 497–508 (2015).
13. J. Ohan, B. Pelle, P. Nath, J.-H. Huang, B. Hovde, M. Vuyisich, A. E. K. Dichosa, S. R. Starkenburg, High-throughput phenotyping of cell-to-cell interactions in gel microdroplet pico-cultures. *Biotechniques* **66**, 218–224 (2019).
14. S. Takahashi, S. M. Whitney, M. R. Badger, Different thermal sensitivity of the repair of photodamaged photosynthetic machinery in cultured *Symbiodinium* species. *Proc. Natl. Acad. Sci. U.S.A.* **106**, 3237–3242 (2009).
15. M. J. Doughty, pH dependent spectral properties of sodium fluorescein ophthalmic solutions revisited. *Ophthalmic Physiol. Opt.* **30**, 167–174 (2010).
16. H. C. Wu, D. Dissard, E. Douville, D. Blamart, L. Bordier, A. Tribollet, F. Le Cornec, E. Pons-Branchu, A. Dapoigny, C. E. Lazareth, Surface ocean pH variations since 1689 CE and recent ocean acidification in the tropical South Pacific. *Nat. Commun.* **9**, 2543 (2018).
17. F. Lyu, L. R. Blauch, S. K. Y. Tang, Quantifying phenotypes in single cells using droplet microfluidics, in *Methods in Cell Biology* (Elsevier Inc., ed. 1, 2018); http://dx.doi.org/10.1016/bs.mcb.2018.09.006, vol. 148, pp. 133–159.
18. N. M. Toriello, E. S. Douglas, N. Thaitrong, S. C. Hsiao, M. B. Francis, C. R. Bertozzi, R. A. Mathies, Integrated microfluidic bioprocessor for single-cell gene expression analysis. *Proc. Natl. Acad. Sci. U.S.A.* **105**, 20173–20178 (2008).
19. L. Kelbauskas, H. Glenn, C. Anderson, J. Messner, K. B. Lee, G. Song, J. Houkal, F. Su, L. Zhang, Y. Tian, H. Wang, K. Bussey, R. H. Johnson, D. R. Meldrum, A platform for high-throughput bioenergy production phenotype characterization in single cells. *Sci. Rep.* **7**, 45399 (2017).
20. A. Reece, B. Xia, Z. Jiang, B. Noren, R. McBride, J. Oakey, Microfluidic techniques for high throughput single cell analysis. *Curr. Opin. Biotechnol.* **40**, 90–96 (2016).
21. N. R. Baker, Chlorophyll fluorescence: A probe of photosynthesis *in vivo*. *Annu. Rev. Plant Biol.* **59**, 89–113 (2008).
22. P. Wang, L. Robert, J. Pelletier, W. L. Dang, F. Taddei, A. Wright, S. Jun, Robust growth of *Escherichia coli*. *Curr. Biol.* **20**, 1099–1103 (2010).
23. M. A. Coffroth, S. R. Santos, Genetic diversity of symbiotic dinoflagellates in the genus *Symbiodinium*. *Protist* **156**, 19–34 (2005).
24. S. Takahashi, S. Whitney, S. Itoh, T. Maruyama, M. Badger, Heat stress causes inhibition of the *de novo* synthesis of antenna proteins and photobleaching in cultured *Symbiodinium*. *Proc. Natl. Acad. Sci. U.S.A.* **105**, 4203–4208 (2008).
25. V. Takhaveev, M. Heinemann, Metabolic heterogeneity in clonal microbial populations. *Curr. Opin. Microbiol.* **45**, 30–38 (2018).
26. E. M. Díaz-Almeyda, C. Prada, A. H. Ohdera, H. Moran, D. J. Civitello, R. Iglesias-Prieto, T. A. Carlo, T. C. LaJeunesse, M. Medina, Intraspecific and interspecific variation in thermotolerance and photoacclimation in *Symbiodinium* dinoflagellates. *Proc. Biol. Sci.* **284**, 20171767 (2017).
27. K. Petrou, D. A. Nielsen, P. Heraud, Single-cell biomolecular analysis of coral algal symbionts reveals opposing metabolic responses to heat stress and expulsion. *Front. Mar. Sci.* **5**, 110 (2018).
28. D. A. Nielsen, K. Petrou, R. D. Gates, Coral bleaching from a single cell perspective. *ISME J.* **12**, 1558–1567 (2018).
29. K. L. Barott, A. A. Venn, S. O. Perez, S. Tambutté, M. Tresguerres, Coral host cells acidify symbiotic algal microenvironment to promote photosynthesis. *Proc. Natl. Acad. Sci. U.S.A.* **112**, 607–612 (2015).
30. A. A. Bulychev, I. Foissner, Pathways for external alkalinization in intact and in microwounded Chara cells are differentially sensitive to wortmannin. *Plant Signal. Behav.* **12**, e1362518 (2017).
31. A. E. Lane, J. E. Burris, Effects of environmental pH on the internal pH of *Chlorella pyrenoidosa*, *Scenedesmus quadricauda*, and *Euglena mutabilis*. *Plant Physiol.* **68**, 439–442 (1981).
32. Z. Lin, L. Wang, M. Chen, J. Chen, The acute transcriptomic response of coral-algae interactions to pH fluctuation. *Mar. Genomics*. **42**, 32–40 (2018).
33. P. M. Rosado, D. C. A. Leite, G. A. S. Duarte, R. M. Chaloub, G. Jospin, U. Nunes da Rocha, J. P. Saraiva, F. Dini-Andreote, J. A. Eisen, D. G. Bourne, R. S. Peixoto, Marine probiotics: Increasing coral resistance to bleaching through microbiome manipulation. *ISME J.* **13**, 921–936 (2019).
34. E. F. Camp, M. R. Nitschke, R. Rodolfo-Metalpa, F. Houlbreque, S. G. Gardner, D. J. Smith, M. Zampighi, D. J. Suggett, Reef-building corals thrive within hot-acidified and deoxygenated waters. *Sci. Rep.* **7**, 2434 (2017).
35. E. Trampe, J. Kolbowski, U. Schreiber, M. Kühl, Rapid assessment of different oxygenic phototrophs and single-cell photosynthesis with multicolour variable chlorophyll fluorescence imaging. *Mar. Biol.* **158**, 1667–1675 (2011).
36. A. Kanazawa, G. J. Blanchard, M. Szabó, P. J. Ralph, D. M. Kramer, The site of regulation of light capture in *Symbiodinium*: Does the peridinin-chlorophyll a-protein detach to regulate light capture? *Biochim. Biophys. Acta* **1837**, 1227–1234 (2014).

Acknowledgments: We acknowledge the help of the Scientific Center for Optical and Electron Microscopy (ScopeM) at ETHZ and of R. Naisbit with scientific editing. **Funding:** L.B. was supported by grants from the Independent Research Fund Denmark (DFF-1323-00747 and DFF-1325-00069), the Swedish Research Council (2019-04401), and the Science for Life Laboratory. M.K. was supported by grants from the Carlsberg Foundation and the Independent Research Fund Denmark (DFF-1323-00065B, DFF-8021-00308B, and DFF-8022-00301B). R.S. acknowledges support from the Gordon and Betty Moore Foundation through a Marine Microbial Initiative Investigator Award (grant 3783) and from the Simons Foundation (grant 542395), as part of the Principles of Microbial Ecosystems (PriME) Collaborative. **Author contributions:** L.B., R.S., and M.K. designed the experiments. L.B. performed laboratory analysis using PhenoChip. L.B., E.L.T., and M.K. optimized PAM use for PhenoChip. M.M.S. performed CFD modeling. L.B., V.I.F., M.K., and R.S. discussed and analyzed the resulting data. K.S.L. helped with initial tests on Raman microscopy. L.B. and R.S. wrote the manuscript. **Competing interests:** The authors declare that they have no competing interest. **Data and materials availability:** All data needed to evaluate the conclusions in the paper are present in the paper and/or the Supplementary Materials. Additional data related to this paper may be requested from the authors.

Submitted 18 February 2020
Accepted 17 July 2020
Published 2 September 2020
10.1126/sciadv.abb2754

Citation: L. Behrendt, M. M. Salek, E. L. Trampe, V. I. Fernandez, K. S. Lee, M. Kühl, R. Stocker, PhenoChip: A single-cell phenomic platform for high-throughput photophysiological analyses of microalgae. *Sci. Adv.* **6**, eabb2754 (2020).

Science Advances

PhenoChip: A single-cell phenomic platform for high-throughput photophysiological analyses of microalgae

Lars Behrendt, M. Mehdi Salek, Erik L. Trampe, Vicente I. Fernandez, Kang Soo Lee, Michael Kühl and Roman Stocker

Sci Adv **6** (36), eabb2754.
DOI: 10.1126/sciadv.abb2754

Science Advances (ISSN 2375-2548) is published by the American Association for the Advancement of Science, 1200 New York Avenue NW, Washington, DC 20005. The title *Science Advances* is a registered trademark of AAAS.